Appl Phys B (2012) 107:659–663
DOI 10.1007/s00340-012-5053-2

Applied Physics B
Lasers and Optics

RAPID COMMUNICATION

Si homojunction structured near-infrared laser based on a phonon-assisted process

T. Kawazoe · M. Ohtsu · K. Akahane · N. Yamamoto

Received: 18 April 2012 / Published online: 25 May 2012
© The Author(s) 2012. This article is published with open access at Springerlink.com

Abstract We fabricated several near-infrared Si laser devices (wavelength ∼1300 nm) showing continuous-wave oscillation at room temperature by using a phonon-assisted process induced by dressed photons. Their optical resonators were formed of ridge waveguides with a width of 10 μm and a thickness of 2 μm, with two cleaved facets, and the resonator lengths were 250–1000 μm. The oscillation threshold currents of these Si lasers were 50–60 mA. From near-field and far-field images of the optical radiation pattern, we observed the high directivity which is characteristic of a laser beam. Typical values of the threshold current density for laser oscillation, the ratio of powers in the TE polarization and TM polarization during oscillation, the optical output power at a current of 60 mA, and the external differential quantum efficiency were 1.1–2.0 kA/cm^2, 8:1, 50 μW, and 1 %, respectively.

Because silicon (Si) is an indirect-transition-type semiconductor, it is difficult to use it as a material for optical devices such as light-emitting diodes (LEDs) and lasers. Nevertheless, Si has been the subject of extensive research for use in fabricating lasers since it shows excellent compatibility with electronic devices [1]. For example, there are reports in the literature on Raman lasers [2] and lasers utilizing quantum size effects [3]; however, parameters such as the operating temperature, efficiency, wavelength and so forth are still not adequate for practical adoption of these devices. To solve these problems, in the research described here, we developed a Si laser showing continuous-wave operation at room temperature. To do so, we applied the same fabrication method and operating principle used for a Si-LED that we previously developed, which used a Si crystal having a p–n homojunction [4]. We report the results here.

Similar to the fabrication of Si LEDs that we have already reported, in this work, first we formed a p–n homojunction by introducing a p dopant into an n-type Si substrate by ion implantation. Then, while irradiating the structure with light, we applied an electrical current to generate Joule heating, causing annealing. Stimulated emission was produced via a two-step transition process driven by the light irradiation. This process is described below [4, 5].

(i) First step: Dressed photons are generated by the light irradiation in regions where the dopant concentration in the p–n junction has a non-uniform spatial distribution. A dressed photon is a quasi-particle representing a coupled state due to the mutual interaction between a photon and an electron on the nanometer scale. The dressed photon then couples with a multi-mode phonon, generating stimulated emission that causes a conduction-band electron to transition from an initial state $|E_{ex}; el\rangle \otimes |E_{ex_{thermal}}; phonon\rangle$ to an intermediate state $|E_g; el\rangle \otimes |E_{ex}; phonon\rangle$. Here, $|E_{ex}; el\rangle$ and $|E_g; el\rangle$ respectively represent the excited state (conduction band) and ground state (valence band) of the

T. Kawazoe (✉) · M. Ohtsu
Department of Electrical Engineering and Information Systems, Graduate School of Engineering, The University of Tokyo, 2-11-16 Yayoi, Bunkyo-ku, Tokyo 113-8656, Japan
e-mail: kawazoe@ee.t.u-tokyo.ac.jp
Fax: +81-3-58411140

T. Kawazoe · M. Ohtsu
Nanophotonics Research Center, Graduate School of Engineering, The University of Tokyo, 2-11-16 Yayoi, Bunkyo-ku, Tokyo 113-8656, Japan

K. Akahane · N. Yamamoto
National Institute of Information and Communications Technology, Koganei, Tokyo 184-8795, Japan

electron; $|E_{ex_{thermal}}; phonon\rangle$ and $|E_{ex}; phonon\rangle$ respectively represent the thermal equilibrium state and excited state of the phonon; and the symbol $\otimes$ represents the direct product of the ket vectors. Because this transition is an electric-dipole–allowed transition, propagating light and a dressed photon are generated.

(ii) Second step: A transition from the intermediate state $|E_g; el\rangle \otimes |E_{ex}; phonon\rangle$ to the final state $|E_g; el\rangle \otimes |E_{ex'}; phonon\rangle$ occurs, producing stimulated emission. Here, $|E_{ex'}; phonon\rangle$ is the excited state of the phonon, but it differs from $|E_{ex}; phonon\rangle$ in process (i) above. Because this is an electric-dipole–forbidden transition, only a dressed photon is generated. After this transition, the phonon relaxes to the thermal equilibrium state.

The two-step transition process described above, referred to as a phonon-assisted process, has already been applied to photochemical vapor deposition [6], photolithography [7], photoetching [8], optical frequency up-conversion [9], photovoltaic devices [10], and so on.

When the electron number densities in the initial state $|E_{ex}; el\rangle \otimes |E_{ex_{thermal}}; phonon\rangle$ and the intermediate state $|E_g; el\rangle \otimes |E_{ex}; phonon\rangle$, n_{ex} and n_{inter}, satisfy the Bernard–Duraffourg inversion condition ($n_{ex} > n_{inter}$) [11], optical amplification gain occurs. In Si, which is an indirect-transition-type semiconductor, the spontaneous emission probability is low, and the probability of the first-step transition in process (i) occurring in the absence of externally incident light is low. However, if the fabricated devices have an optical cavity structure for confining the emission energy in the p–n junction, and if the optical amplification gain is larger than the cavity loss, there is a possibility of laser oscillation occurring as a result of spontaneous emission.

To examine this possibility, we fabricated Si lasers by the following method. We used an As-doped n-type Si crystal with an electrical resistivity of 10 Ω cm and a thickness of 625 μm as a device substrate. This substrate was doped with boron (B) by ion implantation to form a p-type layer. The implantation energy for the B doping was 700 keV, and the ion dose density was 5×10^{13} cm^{-2}. After forming a p–n homojunction, an indium tin oxide (ITO) film with a thickness of 150 nm was deposited on the p-layer side of the Si substrate, and an aluminum (Al) film with a thickness of 80 nm was deposited on the n-substrate side, both by RF sputtering, for use as electrodes. Next, the Si substrate was diced to form the device. The device area was about 400 mm^2. Similarly to [4], the substrate was irradiated with laser light having a wavelength of 1320 nm and a power density of 200 mW/cm^2, during which annealing was performed by applying a forward-bias current of 1.2 A to generate Joule heating, causing the B to disperse.

With this method, the spatial distribution of the B concentration changes, forming microdomain boundaries in a self-organized manner, which allows efficient generation of the phonon-assisted process. These domain boundaries have a shape and distribution suitable for efficiently inducing the phonon-assisted process described above during light emission [4, 5].

Next, to fabricate a Si laser, the ITO electrode and the Al electrode on the Si substrate were removed by etching. Then, the ridge waveguide structure was fabricated by using conventional photolithography. An SiO_2 film, used as a mask in wet chemical etching of Si by KOH, was deposited by means of tetraethyl orthosilicate chemical vapor deposition (TEOS-CVD). After transferring the mask pattern, with a line width of 10 μm, to the SiO_2, KOH etching was conducted to fabricate a ridge waveguide structure with a depth of 2 μm. Then, an SiO_2 film for isolating the Si wafer and the electrode was deposited by TEOS-CVD, and a contact window was formed on top of the ridge waveguide. After that, an Al electrode was deposited by DC sputtering. The substrate was then polished to a thickness of 100 μm, and Al was deposited on the reverse side of the Si substrate. The sample was cleaved to various cavity lengths, and the cleaved facets served as mirrors. We fabricated several Si laser devices with the above method. Note that all of the experiments described below were conducted at room temperature (15–25 °C).

Figure 1(a) illustrates the device structure. From secondary ion mass spectrometry (SIMS) measurements, we confirmed that the active layer formed in the p–n junction was located at a depth of 1.5–2.5 μm from the surface of the Si substrate. This corresponds to the bottom of the ridge waveguide. Figure 1(b) shows optical micrographs of a fabricated Si laser. The width and thickness of the ridge waveguide constituting the resonator were 10 μm and 2 μm, respectively. We fabricated several Si lasers with resonator lengths of 250–1000 μm. The guiding loss in the ridge waveguide and the optical scattering loss at the cleaved facets were estimated to be about 70 % for the TE-polarization component. Because this ridge waveguide does not exhibit optical confinement in the thickness direction, the guiding loss is large; it can be estimated to be 90 % or more. However, because an active layer that efficiently generates dressed photons is formed in the p–n junction by the phonon-assisted annealing process, the effective refractive index of the active layer is higher than the refractive index of the surrounding area. Therefore, the actual guiding loss is smaller than the above value. We measured the current density dependency of the optical amplification gain resulting from irradiating the Si laser with 1320 nm-wavelength laser light and obtained a transparent current density of $J_{tr} = 26.3$ A/cm^2. This value is about 1/10 of that for a conventional laser device made using a direct-transition-type semiconductor [12], demonstrating the possibility that this ridge waveguide with the p–n homojunction structure has adequate performance for use as a laser.

Of the several Si lasers that we fabricated, the current–voltage characteristic for the laser with a resonator length

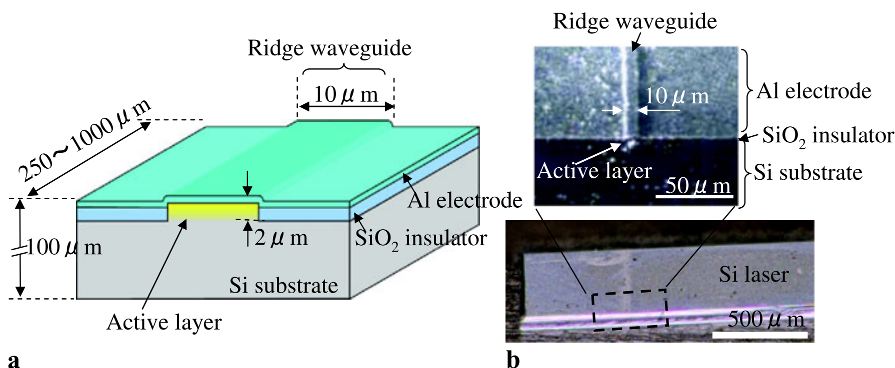

Fig. 1 (**a**) Schematic diagram for explaining structure of fabricated Si lasers. (**b**) Optical micrographs

of 750 μm is shown in Fig. 2(a). The red squares and the blue circles are the results of measurements obtained while increasing the current and decreasing the current, as shown by the red and blue arrows, respectively. In both cases, the voltage value showed a large change at a current value of 50 mA, which corresponds to the threshold current for laser oscillation. This can be explained using the optical radiation pattern of the Si laser. Far-field images of the optical radiation pattern are shown next to numerals ① to ⑤ in Fig. 2(a). A near-field image is also shown next to numeral ③. There is a ridge waveguide with a width of 10 μm at the center of the circle indicated with the white dotted line in this near-field image. At an injection current of 50 mA and above, the optical radiation pattern was concentrated inside the ridge waveguide, and the optical power was increased. This concentration indicates that the directivity of the optical radiation pattern was high due to the laser oscillation. At an injection current below 50 mA, on the other hand, the directivity was low; this is because the main components of the optical radiation pattern are spontaneous emission and amplified spontaneous emission (ASE).

The left side of Fig. 2(b) shows near-field images for the TM- and TE-polarization components forming the optical radiation pattern at ③ in Fig. 2(a). The right side of Fig. 2(b) shows the cross-sectional light intensity profiles taken along the white dotted lines in these near-field images. From these figures, the TM-polarization component from the Si laser was spread over the entire device, whereas the TE-polarization component was concentrated at the location of the ridge waveguide. Because the output beam from a conventional semiconductor laser during oscillation contains the TE-polarization [13], this measurement result also confirms that laser oscillation occurred. In this measurement, the intensity ratio of the TE-polarization and the TM-polarization was 8:1. On the other hand, in a usual semiconductor laser, the intensity ratio of the two polarizations is 100:1 or greater [13]. The reason for the difference between our result and this value is that there is no optical confinement structure in the thickness direction of the ridge waveguide, and also because the spectral wavelength bands of the spontaneous emission and ASE are extremely wide.

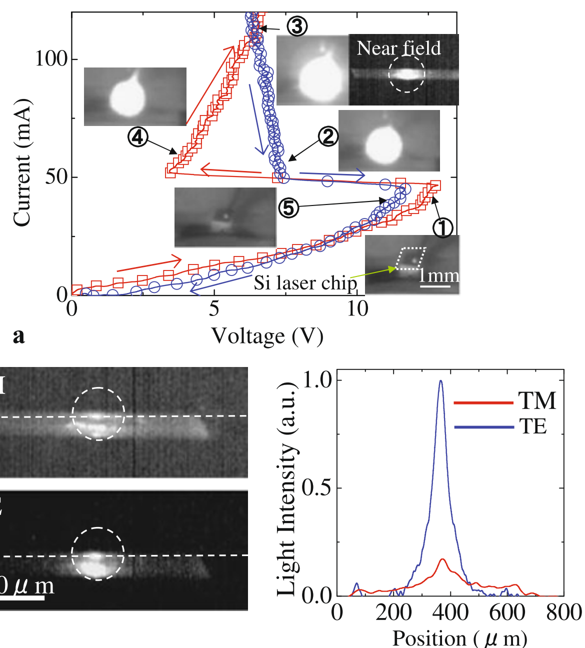

Fig. 2 Images of optical radiation pattern from Si laser (resonator length 750 μm). (**a**) Current–voltage characteristic of Si laser. *Red squares* and *blue circles* are results measured while increasing and decreasing the current, as shown by the *red* and *blue arrows*, respectively. Far-field images of the output optical radiation pattern are shown beside numerals ① to ⑤. A near-field image is also shown beside numeral ③. The *circle* indicated with the white dotted white line shows the ridge waveguide structure. (**b**) The left-hand side shows near-field images of the TM-polarization and TE-polarization in the output light from the Si laser. These correspond to ③ in (**a**). The *circle* indicated with the white dotted white line shows the ridge waveguide structure. The right-hand side shows the cross-sectional light intensity profiles taken along the white dotted lines in the near-field images at the left

Figure 3(a) shows the output light spectral characteristics of the Si laser. In these measurements, in order to separately observe each longitudinal mode, we used a device having a shorter resonator (resonator length 250 μm) than that in Fig. 2. A sharp peak showing laser oscillation at an injection current of 60 mA was observed at 1356 nm (the position indicated by the upward-pointing arrow in the figure); however, the tip of the peak went off the top edge of the graph

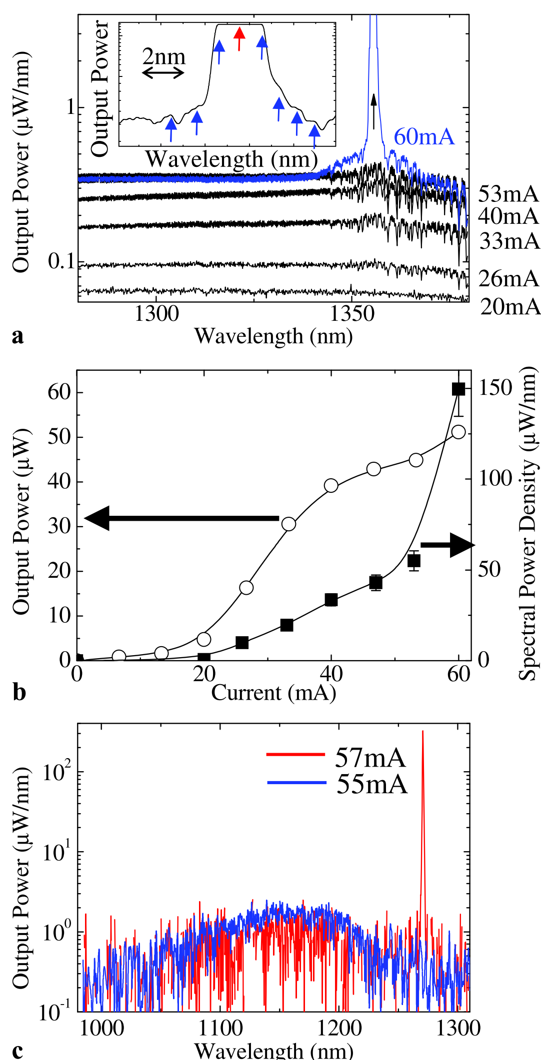

Fig. 3 Spectral characteristics of output light from Si laser. (**a**) Current dependency of output light spectrum (resonator length = 250 μm). The *inset* shows an enlarged view in the vicinity of the peak in the oscillation spectrum during laser oscillation (current = 60 mA). The *upward–pointing arrows* show the positions of the longitudinal modes. (**b**) Current dependency of output optical power. The *white circles* are values obtained by integrating the optical power with respect to wavelength, in the wavelength range 1220–1380 nm. The *black squares* are values of the spectral power density at a wavelength of 1356 nm. (**c**) Output light spectra from Si laser (resonator length 500 μm) above the oscillation threshold (current 57 mA) and below the oscillation threshold (55 mA)

due to saturation of the photo-receiver sensitivity of the measurement equipment. The inset shows a magnified view of the vicinity of the oscillation spectral peak during laser oscillation, where several longitudinal modes (positions indicated by the upward-pointing arrows in the inset) were observed at a wavelength spacing of 1.0 nm, corresponding to the resonator length (250 μm). Figure 3(b) shows the current dependency of the output light power. The white circles are values obtained by integrating the optical power with respect to wavelength in the wavelength range 1220–1380 nm. At an injection current of 60 mA, the optical output power was 50 μW, and the external differential quantum efficiency was 1 %. This value is as high as that reported for a 1.3 μm-wavelength double heterojunction laser using InGaAsP/InP, which is a direct-transition-type semiconductor [14]. The black squares are values of the spectral power density at a wavelength of 1356 nm. At the injection current of 60 mA, the spectral power density was 150 μW/nm. Because this device had a wide emission wavelength band, as the current increases, the optical power of the spontaneous emission and ASE also increase; therefore, the measurement results indicated by the white circles do not show a sudden increase in the optical output power due to laser oscillation. The black squares, on the other hand, do show this, and the threshold current for laser oscillation was found to be 50 mA, giving a threshold current density of 2.0 kA/cm^2.

To measure the optical power and spectral linewidth at the peak wavelength in the laser oscillation spectrum, we measured the output spectrum during laser oscillation (current = 57 mA) using a different Si laser (resonator length = 500 μm) from that used in Figs. 3(a) and 3(b). The results are shown in Fig. 3(c). The vertical axis of this graph is a logarithmic scale. At an injection current of 55 mA or less, only a wide emission spectrum was measured; however, above the threshold current (about 56 mA), a sharp laser oscillation spectrum was observed, with a center wavelength of 1271 nm. The full width at half maximum (FWHM) was the wavelength resolution (0.9 nm) or less. In addition, from these measurement results, we confirmed that the threshold current density for laser oscillation was 1.1 kA/cm^2.

In summary, we fabricated several near-infrared Si lasers (1300 nm wavelength band) showing continuous-wave oscillation at room temperature. For the fabrication and operation of these Si lasers, we used a phonon-assisted process induced by dressed photons. The optical resonators of these lasers were formed of a 10 μm-wide, 2 μm-thick ridge waveguide with two cleaved facets, and the resonator lengths were 250–1000 μm. The oscillation threshold currents of these Si lasers were 50–60 mA. From near-field and far-field images of the optical radiation patterns, we observed the high directivity which is characteristic of a laser beam. Typical values of the threshold current density for laser oscillation, the ratio of powers of the TE-polarization and the TM-polarization during oscillation, the optical output power for a current of 60 mA, and the external quantum efficiency were 1.1–2.0 kA/cm^2, 8:1, 50 μW, and 1 %, respectively.

Open Access This article is distributed under the terms of the Creative Commons Attribution License which permits any use, distribution, and reproduction in any medium, provided the original author(s) and the source are credited.

References

1. D. Liang, J.E. Bowers, Nat. Photonics **4**, 511 (2010)
2. H. Rong, R. Jones, A. Liu, O. Cohen, D. Hak, A. Fang, M. Paniccia, Nature **433**, 725 (2005)
3. S. Saito, Y. Suwa, H. Arimoto, N. Sakuma, D. Hisamoto, H. Uchiyama, J. Yamamoto, T. Sakamizu, T. Mine, S. Kimura, T. Sugawara, M. Aoki, Appl. Phys. Lett. **95**, 241101 (2009)
4. T. Kawazoe, M.A. Mueed, M. Ohtsu, Appl. Phys. B **104**, 747 (2011)
5. K. Kitamura, T. Kawazoe, M. Ohtsu, Appl. Phys. B (2012). doi:10.1007/s00340-012-4991-z
6. T. Kawazoe, K. Kobayashi, S. Takubo, M. Ohtsu, J. Chem. Phys. **122**, 024715 (2005)
7. T. Kawazoe, M. Ohtsu, Y. Inao, R. Kuroda, J. Nanophotonics **1**, 011595 (2007)
8. T. Yatsui, K. Hirata, W. Nomura, Y. Tabata, M. Ohtsu, Appl. Phys. B **93**, 55 (2008)
9. T. Kawazoe, H. Fujiwara, K. Kobayashi, M. Ohtsu, IEEE J. Sel. Top. Quantum Electron. **15**, 1380 (2009)
10. S. Yukutake, T. Kawazoe, T. Yatsui, W. Nomura, K. Kitamura, M. Ohtsu, Appl. Phys. B **99**, 415 (2010)
11. M.G.A. Bernard, G. Duraffourg, Phys. Status Solidi **1**, 699 (1961)
12. W.J. Choi, P.D. Dapkus, J.J. Jewell, IEEE Photonics Technol. Lett. **11**, 1572 (1999)
13. T. Tanbun-Ek, N.A. Olsson, R.A. Logan, K.W. Wecht, A.M. Sergent, IEEE Photonics Technol. Lett. **3**, 103 (1991)
14. Zh.I. Alferov, Semiconductors **32**, 1 (1998)